LA-UR-14-27403
Approved for public release; distribution is unlimited.

Title: Uncertainties of Gamma-Ray Flux into 4Pi

Author(s): Karpius, Peter Joseph
Stange, Sy
Cutler, Theresa E

Intended for: Report

Issued: 2014-09-23

Uncertainties of Gamma-Ray Flux into 4π

P.J. Karpius, S. Stange, T.E. Cutler

Introduction

This paper examines the uncertainties involved in total flux gamma-ray measurements made in the field with large volume high-purity germanium (HPGe) detectors. The photon flux, $\dot{\gamma}$, into 4π steradians (sr) for a particular energy, *E*, can be written as

$$\dot{\gamma}(E)_{4\pi} = \frac{1}{T_l} \times \frac{C_E}{D_E}$$

Here, T_l is the live time of the measurement, C_E is the net area of the respective gamma-ray peak at energy *E*, and D_E is the absolute detector efficiency for energy *E*. If we propagate the errors on the above relation we obtain the following:

$$\sigma_{\dot{\gamma}}^2 = \left(\frac{\partial \dot{\gamma}}{\partial T_l}\right)^2 \sigma_{T_l}^2 + \left(\frac{\partial \dot{\gamma}}{\partial C_E}\right)^2 \sigma_{C_E}^2 + \left(\frac{\partial \dot{\gamma}}{\partial D_E}\right)^2 \sigma_{D_E}^2$$

We will make the assumption that modern data acquisition systems provide accurate and precise values for live time under normal measurement conditions. The uncertainty in the live time and hence the first term above, will therefore be considered negligible. The partial derivatives with respect to the net counts and absolute detector efficiency for the peak at energy *E* are written as

$$\frac{\partial \dot{\gamma}}{\partial C_E} = \frac{1}{T_l D_E}$$

$$\frac{\partial \dot{\gamma}}{\partial D_E} = -\frac{C_E}{T_l {D_E}^2}$$

The uncertainty in the net peak area, σ_{C_E}, and that in the detector efficiency, σ_{D_E}, will be discussed separately.

Uncertainties of Net Peak Areas

It has been suggested that automated peak-fitting routines be used to determine the net areas of peaks in gamma-ray spectra. For clean, good-quality, repeatable data of known nuclide composition, this is not an entirely unreasonable approach. In the practical world however, the data are rarely ideal and a skilled, albeit not infallible, human analyst must be employed to obtain the required net areas for the gamma-ray peaks of interest. The uncertainties on the extracted net peak areas will be written in terms of the following contributions:

$$\sigma_{C_E}^2 = \left(\sigma_{Sfw} + \sigma_{User}\right)^2$$

In the above relation the first term, σ_{Sfw}, refers to the uncertainty returned by the selected software package for the fitted peak. The second term, σ_{User}, refers to the systematic uncertainty incurred by the possibility that different users will, in general, tailor the same peak fit differently and therefore obtain different results for the extracted net area. Note that the above assumes that the two contributions are independent and can be combined directly as shown, which has not been proven. The contributions to the systematic uncertainty represented by the second term may include but are not limited to selections of the boundaries of the spectral region of interest (ROI), whether or not to include low-energy tailing, allowing for a single peak only or a multiplet of peaks to be fit, and the selection of the particular model for the continuum beneath the peak(s) of interest. Examples of some of these sources of uncertainty in a peak fitted "by hand" using the Los Alamos National Laboratory (LANL) software package PeakEasy[i], are shown in Figure 1.

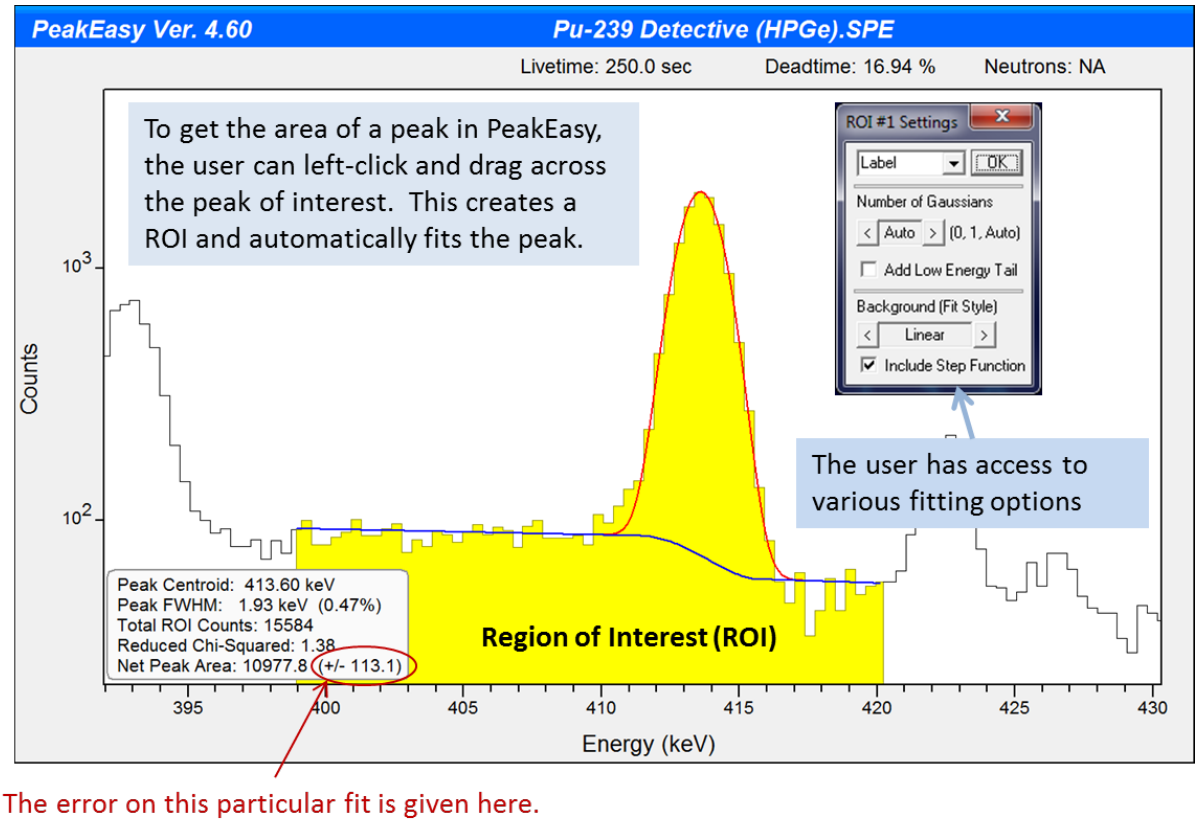

Figure 1: Fitting a gamma-ray peak in PeakEasy. The yellow represents the region of interest selected by the user. A stepped continuum has been selected and is visible beneath the peak, which the algorithm fits with a Gaussian.

Note that the uncertainty on the fitted peak shown in Figure 1 of ±113.1 counts represents σ_{Sfw} in our analysis. In this example, the user has selected a region from 399 keV to just above 420 keV and a linear step-function background, precluded a low-energy tail, and allowed the number of Gaussian peaks in the ROI to float. The uncertainty returned by PeakEasy is only based on statistics and does not account for any uncertainty in the fit itself[ii]. PeakEasy is only one example of available software packages for

peak area determination; currently, it is not mandated that analysts use a particular piece of software or fit gamma-ray peaks in a standard way. Thus, σ_{Sfw}, also inherently includes a contribution from the variation among specific software packages.

An estimate of the systematic user uncertainty, σ_{User}, was determined empirically using a limited data set from skilled analysts fitting the same peaks in the same spectra. In the case of uranium, the Monte Carlo code MCNP[iii] was used to generate spectra where the intensity at each gamma-ray energy was governed only by the energy deposited in the detector and not modified by statistics of charge collection etc. This raw MCNP spectrum essentially contains peaks represented by 'delta functions'[*] on a minimal Compton continuum. The raw spectrum was then 'smeared' to account for instrument-based broadening, by convolving a Gaussian function of the appropriate width at each channel. The total counts in each Gaussian equaled the total counts in the selected channel of the raw spectrum. This smeared spectrum was then submitted to analysts for peak fitting. Real data were used in the case of plutonium due to the added difficulty of incorporating neutron-induced features in the spectrum with MCNP.

Peaks from ^{235}U, ^{239}Pu, and ^{240}Pu were fit by 5 analysts. The results of this study are listed in Table 1. The distributions of the analysts' results for each peak are illustrated by various plots in Appendix A. The uncertainty -weighted average of the extracted net peak areas for each energy was recorded, where the uncertainty used for the weighting was that returned by the software used by each analyst. In general this software was PeakEasy, although for some peaks, such as the 642-keV peak of ^{240}Pu, additional software such as the PuIsotopics[iv] spreadsheet or FRAM[v], both developed at LANL, was required. This is due to the 642-keV peak being generally weak but more importantly, part of a multiplet of peaks that cannot easily be completely deconvoluted.

Table 1: Peak Area Extraction Variation Due to User Fit Settings

Nuclide	Energy [keV]	Mean Area	Mean σ_{Sfw}	|%Δ| from mean	± %Δ from MCNP
^{235}U	144	120749	374	0.084	0.63
^{235}U	186	707583	847	0.19	0.87
^{239}Pu	375	492567	764	1.28	-
^{239}Pu	414	552056	778	0.74	-
^{240}Pu	642	2355	141	7.91	-
^{239}Pu	646	10214	171	3.84	-

The average absolute difference from the mean area for each peak was calculated and is shown in Table 1. Also the net areas extracted for the uranium peaks were compared to simulation results[vi]. The true values for the uranium peak areas were obtained from the raw simulation. From the first two plots in Appendix A (which show the analysts' results for the 144 keV and 186 keV peaks of ^{235}U) and the results in Table 1, we see that there is a positive systematic uncertainty of less than 1% in the results from the analysts compared to each true (MCNP) peak area. The overlapping of adjacent peak and continuum Gaussians from the smearing process likely contributed strongly to the observed systematic uncertainty.

[*] This simulation populated a spectrum of energy-binning appropriate for fielded detectors. Therefore the 'delta function peaks' were actually one channel or energy bin in width.

Also, this discrepancy is only based on the statistical uncertainty given by the software, which may not account for fitting algorithm uncertainties or variation due to differences in fitting software selection.

The variation in results depends greatly on which peak is selected. For example, there is roughly a 1% spread in the results for the two main peaks of the 400-keV region of plutonium and a 4 – 8% spread in the two peaks listed from the 640-keV region. It is important to state, though, that the trend in uncertainty cannot be easily modeled as a function of energy – it is not necessarily true that the fits to higher-energy peaks will show more uncertainty. It must be estimated on a peak-by-peak basis since certain peaks may have interferences or sit atop more complex continua than others and such things cannot themselves be modeled across complex spectra as a function of energy in a straightforward way.

Uncertainties of Absolute Detector Efficiency

The absolute detector efficiency, D_E, accounts for both the solid angle subtended by the detector at the measurement distance, *r*, and the intrinsic efficiency, I_E, of the detector system. The intrinsic detector efficiency characterizes the probability that a photon of a particular energy that is incident on the detector face will make a count in a peak at that energy in the spectrum. The fraction of the solid angle, Ω, subtended by the detector, out of 4π sr can be written in terms of the radius of the detector crystal, *R*, and the measurement distance, *r*.

$$\frac{\Omega}{4\pi} = \frac{1}{2}(1 - \cos\theta) = \frac{1}{2}\left(1 - \cos\left(\arctan\frac{R}{r}\right)\right)$$

This is illustrated in Figure 2.

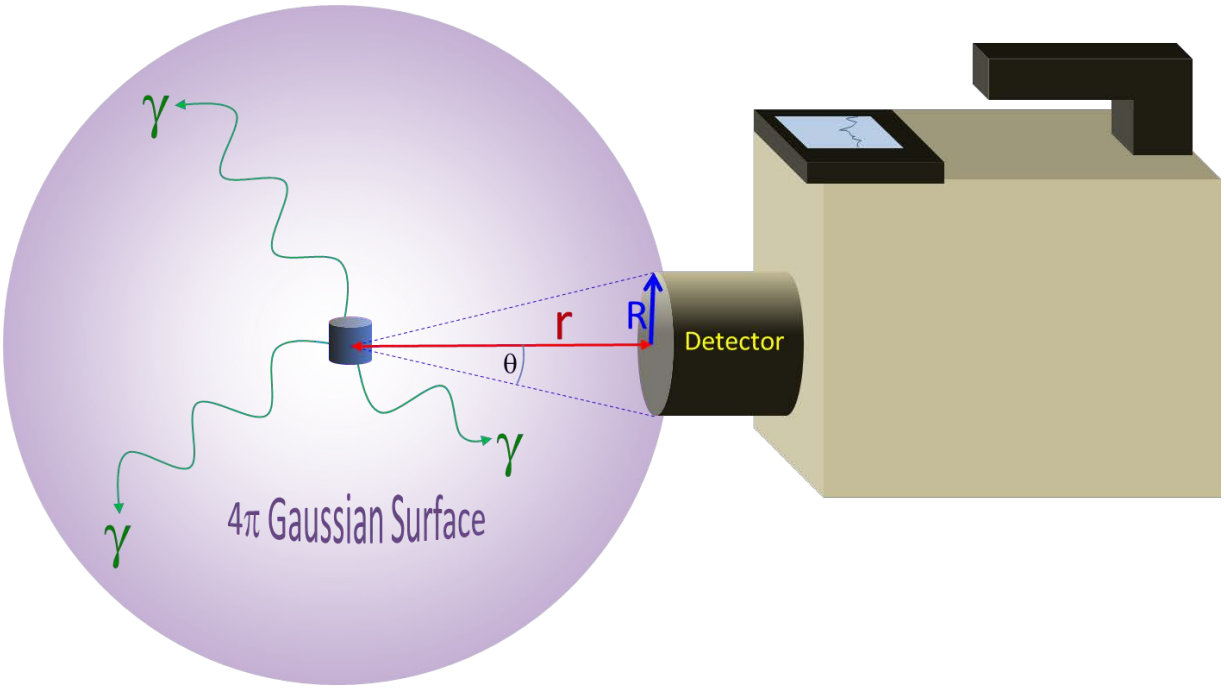

Figure 2: Solid angle subtended by detector of radius R, at distance r from source center.

If the detector efficiency D_E (r_0) is determined at a distance r_0, and the field measurement is conducted at distance r, the absolute detector efficiency, D_E (r), at the latter will be

$$D_E(r) = D_E(r_0)\frac{\Omega}{\Omega_0} = I_E\frac{\Omega}{4\pi}$$

where Ω and Ω_0 are the solid angles of the field measurement and of the efficiency calibration distance, respectively. Note that I_E is the intrinsic detector efficiency at energy E, illustrated in Figure 2, and itself is independent of solid angle. If we make the reasonable assumption that the uncertainties on the calibration distance and the detector radius are negligible[†] then the uncertainty on the absolute detector efficiency only depends on uncertainties in the fit of the intrinsic efficiency curve and field measurement distance.

$$\sigma_{D_E}^2 = \left(\frac{\partial D_E}{\partial I_E}\right)^2 \sigma_{I_E}^2 + \left(\frac{\partial D_E}{\partial r}\right)^2 \sigma_r^2$$

We can write the detector efficiency partial derivatives in terms of the solid angle.

$$\left(\frac{\partial D_E}{\partial I_E}\right)^2 = \left(\frac{\Omega}{4\pi}\right)^2$$

$$\left(\frac{\partial D_E}{\partial r}\right)^2 = \frac{{I_E}^2 R^4/4}{(R^2 + r^2)^3}$$

The uncertainty on the intrinsic efficiency curve, σ_{I_E}, is given by the covariance matrix stated in Appendix B and will be discussed in greater depth below. The field measurement distance, r_r, is often very roughly estimated, so its uncertainty, σ_r, is likely the dominant source of uncertainty overall.

We recall that the intrinsic detector efficiency characterizes the probability that a photon of a particular energy that is incident on the detector face will make a count in a peak at that energy in the spectrum. Ironically, although this concept is entirely independent of measurement conditions outside of the detector itself, it can only be determined by means of an absolute measurement. To obtain the intrinsic efficiency for a particular detector, high-quality measurements of various point sources are conducted for a live time, T_l, at a given distance r_0 (and hence solid angle Ω_0). Peak areas, C_E, at each energy E are normalized by live time and respective branching ratios, BR_E, and activities, Act.

$$D_E(r_0) = \frac{C_E}{BR_E}\frac{1}{T_l}\frac{1}{Act} = I_E\frac{\Omega_0}{4\pi}$$

[†] Although radii of many commercial detectors have non-negligible crystal dimension uncertainties, the fielded large volume HPGe detectors of concern are well characterized.

The data are then fit with a curve, the shape of which represents *relative* efficiency. Relative efficiency, RE_E, is an energy-dependent value that is proportional to the counts in a particular gamma-ray peak normalized by the branching ratio for that peak for its corresponding nuclide[‡].

$$RE_E \propto \frac{C_E}{BR_E}$$

Relative efficiency accounts for external attenuation (between the source and detector), self-attenuation of the source photons by the source matrix, and intrinsic detector efficiency. The proportionality relationship exists because differing activities of different nuclides in a measurement will yield different relative efficiency curves. If all photons from all nuclides in a measurement are attenuated in the same way, then they will all follow the same *shape* of a given relative efficiency curve. An example of a detector intrinsic efficiency calibration is shown in Figure 3.

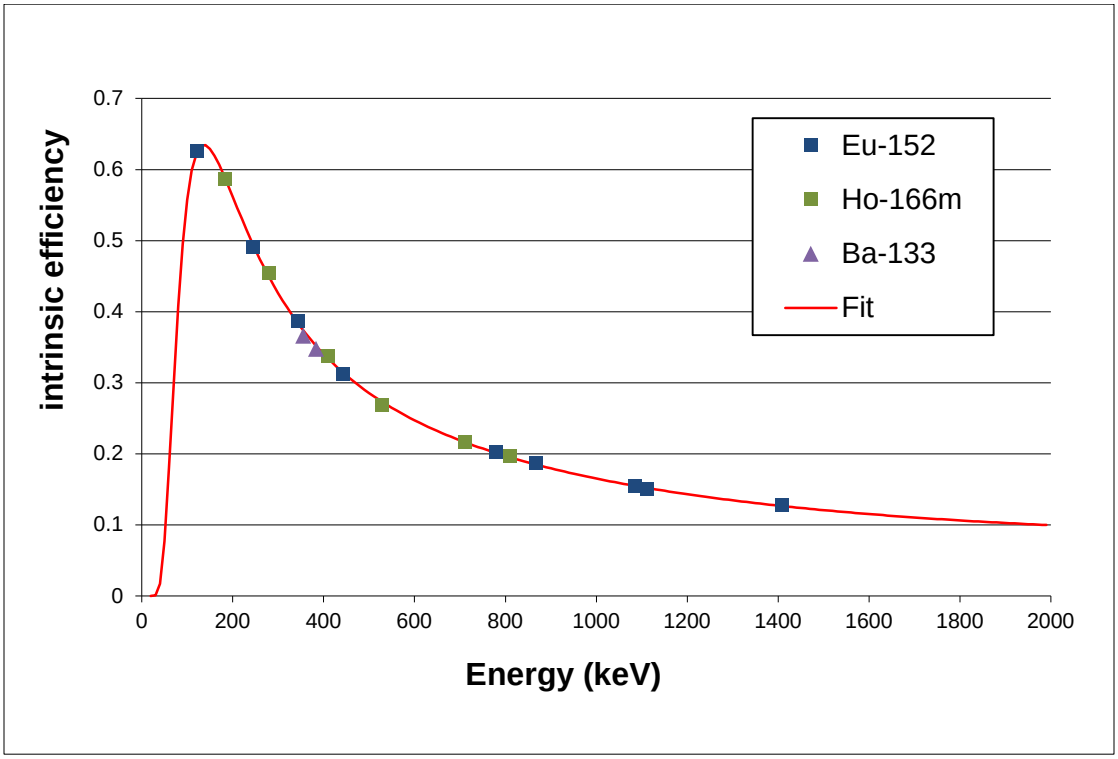

Figure 3: Example of Detector Intrinsic Efficiency Calibration Curve

Calibration sources are selected with gamma-ray peak energies that span the dynamic range of the detector. Half-lives of these sources are sufficiently short that a reasonable signal may be obtained with a small (point-like) amount of source material. This minimizes self-attenuation of the source photons, which, with the limiting of external attenuation to the source encapsulation leaves only the intrinsic detector efficiency governing the shape of the relative efficiency curve.

[‡] Not to be confused with the legacy definition of relative efficiency, which compares a detector's efficiency at 1332 keV (or other energies) to that of a 3"x3" NaI(Tl) detector.

Since the data from each nuclide have been normalized by the respective activity, and all photons are attenuated the same way, the data follow a smooth curve as discussed above. An empirical function in the natural logarithm of the energy can then be used to fit the data.

$$f(E) = e^{\left(c_0 + c_1 \ln E + c_2 (\ln E)^2 + c_3 (\ln E)^3 + c_4 (\ln E)^4 + c_5 (\ln E)^5\right)}$$

The uncertainty of the fit of the detector intrinsic efficiency σ_{I_E}, can be written in terms of the sum over the product of the square of the fitting function and the *linearized*[§] variances and covariances of the fitting parameters.

$$\sigma_{I_E}^2 = \sum_{k,l} f(E)^2 \sigma_{kl}'^2$$

The mathematical derivation of this uncertainty is shown in Appendix B.

Combining this with our previous results we obtain the following already simplified but still less-than-elegant expression for the variance of the flux of photons into 4π sr.

$$\sigma_{\dot{\gamma}}^2 = \left(\frac{\sigma_{C_E}}{T_l D_E}\right)^2 + \left(\frac{C_E}{T_l {D_E}^2}\right)^2 \underbrace{\left[\left(\frac{\Omega}{4\pi}\right)^2 \underbrace{\sum_{k,l} f(E)^2 \sigma_{kl}'^2}_{\sigma_{I_E}^2} + \left(\frac{{I_E}^2 R^4/4}{(R^2 + r^2)^3}\right)\sigma_r^2\right]}_{\sigma_{D_E}^2}$$

The uncertainties on the data points used to determine intrinsic detector efficiency arise from the very same sources, σ_{Sfw} and σ_{User}, whose contribution to the uncertainty of net peak areas in field measurements was discussed earlier. Normally, however, calibration data are of better quality than field measurements in terms of longer count durations and reasonable dead times, which yields better statistics with good resolution. Furthermore gamma-ray peaks chosen for calibration purposes are generally clean in the sense that they are isolated (singlets) sitting atop reasonable continua. These factors will minimize net peak area uncertainties. We will therefore not consider user-to-user variation, σ_{User}, in peak area uncertainties for calibration data.

We have already stated the importance of distance on the uncertainty of total photon flux. The degree of uncertainty in the determination of distance depends in part on whether a measurement is conducted in the near field or in the far field. We define near field to be a source-to-detector distance that is on the order of or less than both the dimensions of the source and the detector. Conversely, the far field represents measurement distances that are larger than both source and detector dimensions. In practice we only measure the distance from the source to the detector *face*. We must also consider the dependence on energy of the effective depth at which gamma-rays interact in the detector crystal,

[§] The primed convention of Bevington[x] has been used to indicate factors modified for linearization.

which is illustrated in Figure 4. Let us define the "total distance" as the distance from the (point) source to the location of interaction in the detector crystal. For small source-to-detector-face (near-field) distances the interaction depth can be a significant fraction of the total distance. In this case, if the source-to-detector distance is assumed to be the same for all energies, then the calculation of both the absolute and intrinsic efficiency will be incorrect because the total distances are energy-dependent.

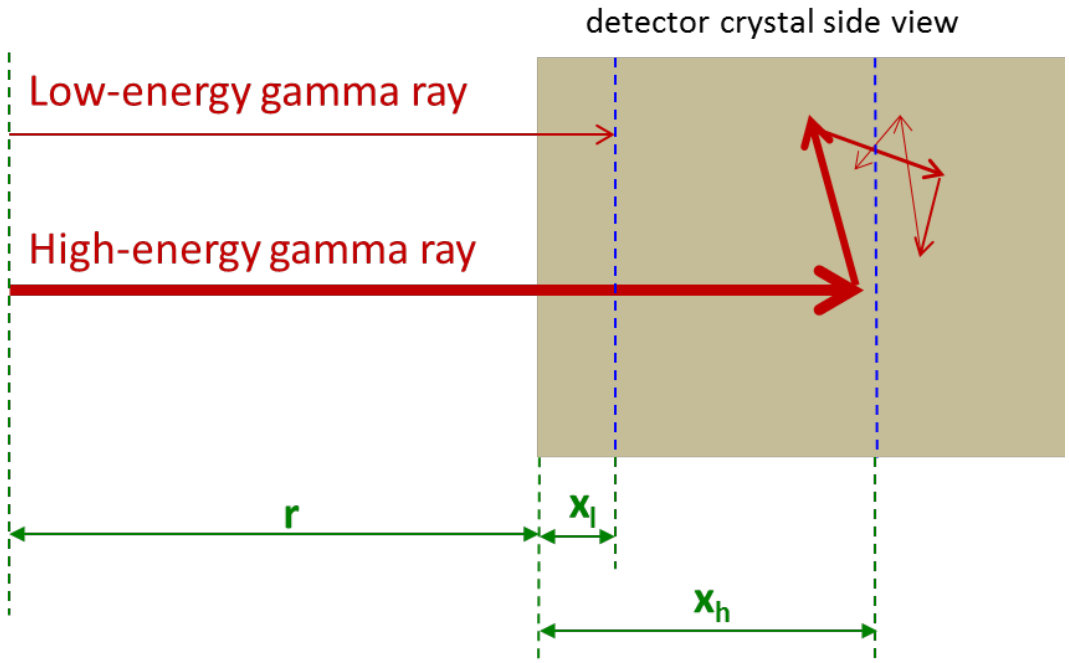

Figure 4: Effective interaction depth of gamma rays in a detector crystal. Here, *r* is the source-to-detector-face distance, x_l and x_h are pictorial low and high-energy interaction depths respectively

In very naïve terms, if we define the effective interaction depth as that which results in a transmission of $1/e$[**] then one mean free path is equal to $1/(\mu\rho)$, where μ is the mass attenuation coefficient and ρ is density of the detector crystal, in this case germanium. The mean free path for 186-keV photons in germanium is ~ 1 cm vs ~5 cm for 2614-keV photons. Consider that at a nominal measurement distance of 50 cm, which would place us in the far field, a deviation in interaction depth of 4 cm will result in a change in solid angle fraction by ~17%. In the near field, the complexities of this are manifested and their effect is magnified greatly. For instance, the data in Figure 5 represent the intrinsic detector efficiency of a 40% HPGe detector measured at a variety of distances between the source and detector face[vii].

[**] Here '*e*' represents Euler's Number. $e \approx 2.71828$

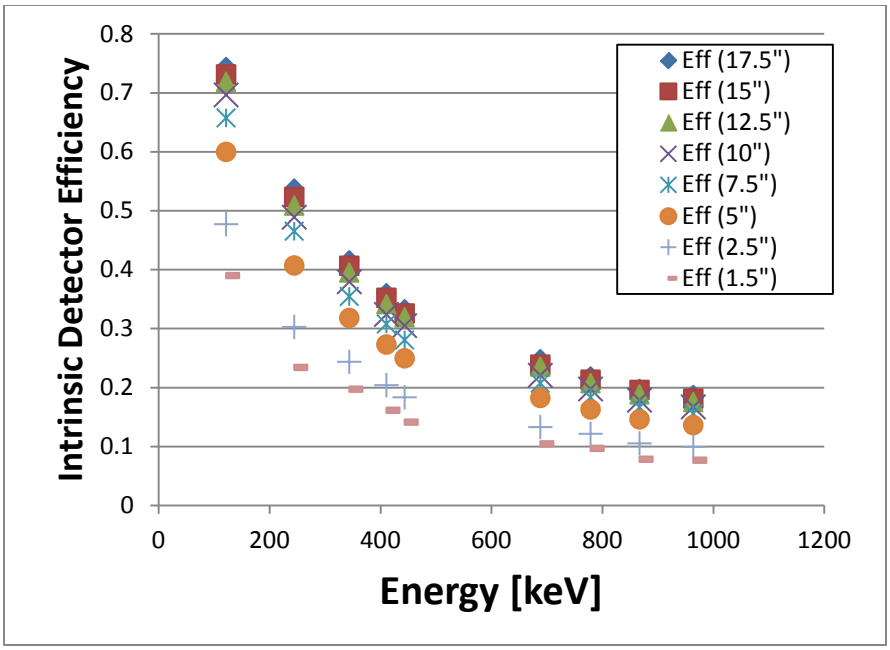

Figure 5: Intrinsic efficiency for a particular 40% HPGe detector as a function of distance between source and detector face

Across the dynamic range of calibration, the efficiency determined at the 1.5" distance is approximately 50-60% lower than the efficiency at 17.5". A rigorous albeit tedious manner in which to address this is to determine intrinsic efficiencies for a variety of applicable detectors over a wide range of measurement distances ranging from the near field to the far field.

At this time the contribution to the uncertainty concerning the effective interaction depth will only be estimated using the comparison of the 17.5" data and the 15" data discussed above, since the measurements about which this paper is concerned are likely to be at distances similar to those that correspond to the far field, such as these numbers suggest. With the understanding that the detector used in the above study is much smaller than a typical (~140%) fielded detector, this very rough estimate yields a ~1-3% uncertainty from the 120 – 1000-keV energy range. For simplicity we will apply a 2% uncertainty $\sigma_{IE(depth)}$ to the intrinsic efficiency across the spectrum. Future work would possibly include conducting a characterization study such as the above for all detectors used in field operations.

It should be noted it is possible for detector intrinsic efficiencies to change over time[viii]. Systematic effects from this may be strong contributors to this uncertainty analysis. However, as we currently have no characterization data illustrating how detector efficiency changes over time we have no means of estimating it at present and it will therefore not be considered.

Illustrating the Methodology

To illustrate the methodology, we now apply the above uncertainty analysis to an example of a spectrum of a plutonium item taken with a known detector at a known distance. The inferred quantities will be the photon flux into 4π for the 375 and 414-keV lines from ^{239}Pu.

Peak Fits: The 400-keV region of the spectrum for this measurement is shown in Figure 6. The 375-keV and 414-keV peaks have been manually fit using PeakEasy Version 4.60. By 'manually fit' we indicate that the user manipulated the ROI boundaries and fitting conditions rather than using the 'double-click' option in PeakEasy, which is essentially a one-step peak fitting method that uses default fitting conditions[††]. A low-energy tail and step function model for the continuum have been selected for both peaks. The region of interest in each case extends well beyond the boundaries of the peak of interest itself. This is to allow the fitting routine to more accurately model the continuum. Such tailoring is also an illustration of the user subjectivity in this method.

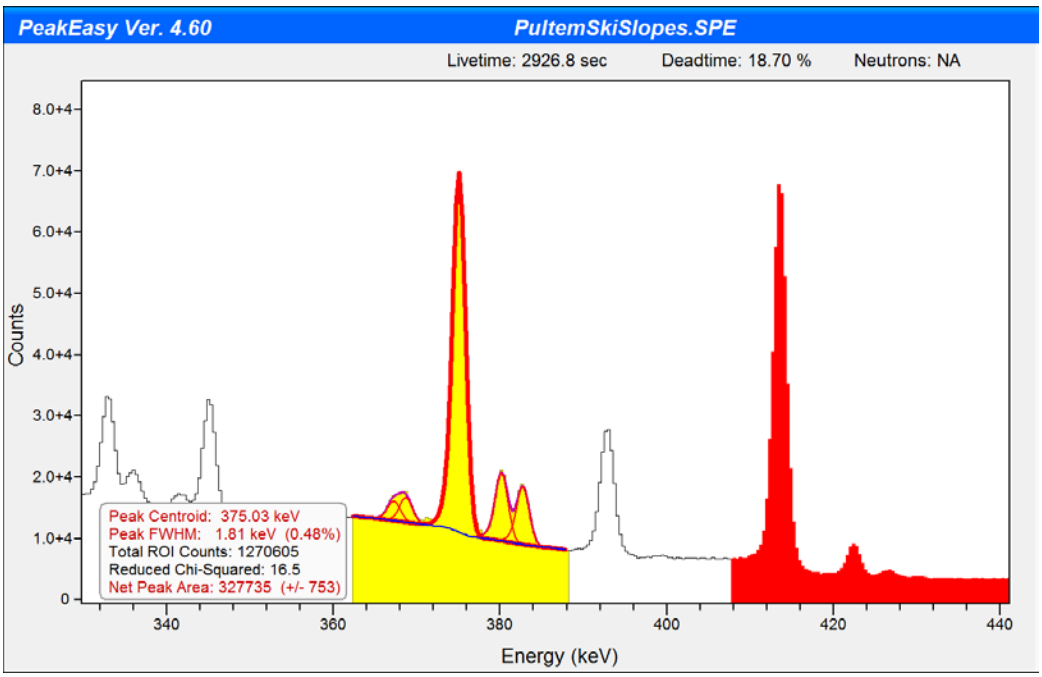

Figure 6: 400-keV region of a plutonium spectrum measured with LANL HPGe Detector "S"

The net areas returned by the software for the 375 and 414-keV peak were 327735 ± 753 and 361603 ± 701 counts respectively. Applying the results of Table 1 to the energy range of interest in a very rough fashion we include the empirical user uncertainty of 1%, or an additional 3277 and 3616 counts to the uncertainties of the 375 and 414-keV peaks, respectively.

Detector: LANL Detector "S" (156%). We apply the previously described method of intrinsic efficiency calibration to this detector using data that were recorded at LANL and are provided in the detector characterization folder of the distribution of Sandia National Laboratories' GADRAS analysis software version 18.4.2[ix]. The radius of the crystal is 4.59 cm.

Distance: For purposes of illustration we will assume a distance from the center of the source to the face of the detector to be 50 cm with an arbitrary 10% uncertainty of σ_r = 5 cm.

For this distance and detector our solid angle fraction $\Omega/4\pi$ is 2.09E-03. The energy-independent inputs to the analysis are compiled in Table 2.

[††] The default parameters for fitting peaks via the 'double-click' method in PeakEasy as of version 4.60 are: single Gaussian only, linear continuum, no low-energy tail.

Table 2: Energy Independent Quantities

Quantity	Value
Distance *r*	50 cm
Distance Uncertainty σ_r	5 cm
Detector radius *R*	4.59 cm
Solid Angle Fraction $\Omega/4\pi$	2.09E-03
Live Time	2926.8 sec

From the approach described above, the intrinsic and absolute detector efficiencies and associated uncertainty for each of the two energies are shown in Table 3 along with the respective partial derivatives. Here we also list the absolute values corresponding to the relative uncertainty of 2% on the intrinsic efficiency due to the effective interaction depth based on the discussion that concerns Figure 5.

Table 3: Detector Efficiency Quantities

Energy	I_E	$\sigma_{IE(fit)}$	$\sigma_{IE(depth)}$	$\sigma_{IE(total)}$	D_E	σ_{DE}	$\left(\frac{\partial\dot{\gamma}}{\partial D_E}\right)^2$
375.0	4.13E-01	3.70E-03	8.26E-03	1.20E-02	8.63E-04	3.02E-08	2.26E16
413.7	4.03E-01	3.61E-03	8.06E-03	1.17E-02	8.42E-04	2.87E-08	3.04E16

The extracted peak areas and their associated uncertainties, including the estimated user-to-user uncertainty estimated in the discussion following Table 1, and the respective partial derivatives, are outlined in Table 4.

Table 4: Peak Area Quantities

Energy	C_E	$\sigma_{CE(sfw)}$	$\sigma_{CE(user)}$	$\sigma_{CE(total)}$	$\left(\frac{\partial\dot{\gamma}}{\partial C_E}\right)^2$
375.0	327735	753	3277	4030	1.57E-01
413.7	361603	701	3616	4317	1.65E-01

The contribution of the two flux uncertainty terms to the total uncertainty is outlined in Table 5 prior to taking the square root. It is quite clear that Term 2, which illustrates the dependence on the absolute detector efficiency, is the dominant factor.

$$\sigma_{\dot{\gamma}}^2 = \underbrace{\left(\frac{\partial\dot{\gamma}}{\partial C_E}\right)^2 \sigma_{C_E}^2}_{Term\ 1} + \underbrace{\left(\frac{\partial\dot{\gamma}}{\partial D_E}\right)^2 \sigma_{D_E}^2}_{Term\ 2}$$

Table 5: Flux Uncertainty Term Influence

Energy	σ_{Flux} Term 1	σ_{Flux} Term 2
375.0	2.55E6	6.82E8
413.7	3.07E6	8.72E8

We display the results for the calculated flux and overall uncertainties for each of the two selected energies in Table 6.

Table 6: Flux and Uncertainty Final Result

Energy	Flux	σ_{Flux}	% Uncertainty
375.0	1.30E5	2.62E4	20.2
413.7	1.47E5	2.96E4	20.2

For our arbitrarily selected input criteria above we obtain relative uncertainties of approximately 20 % on the flux for the gamma lines at 375 and 414 keV.

In the above analysis we have attempted to capture all of the non-negligible contributors to the uncertainty on the calculated photon flux. We now further investigate the dominant components of the final uncertainty. In practice we will more than likely be using a well-characterized detector that has a relatively small uncertainty for its intrinsic efficiency. Furthermore, the measurement is quite likely to be in the far field, making the source-to-detector-face distance large when compared with the detector crystal depth. These two things would, in a relative sense, mitigate the uncertainty due to the intrinsic detector efficiency and the effective depth of the crystal. The two remaining sources of significant uncertainty then would be the extracted net peak areas and the absolute detector efficiency, or more specifically the solid angle, which depends on the measurement distance. In Figure 7 we compare the effect of an uncertainty in these two parameters on the overall uncertainty on the calculated flux for the 414-keV peak of the above example. The displayed result of this calculation might seem obvious but we retain it for clarity.

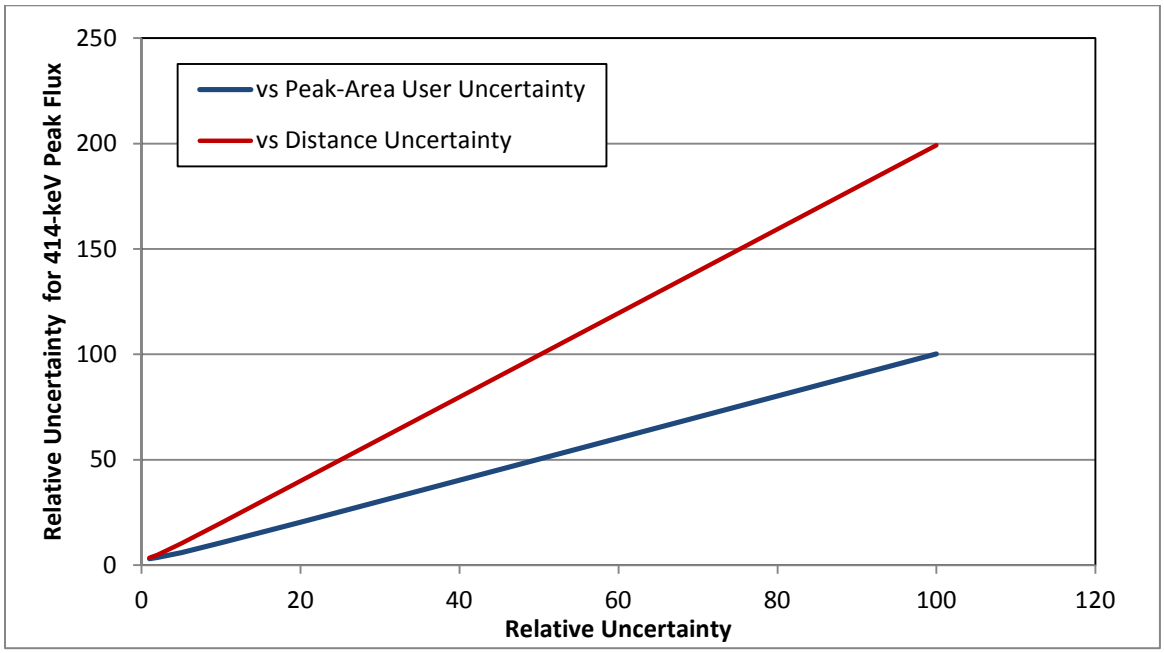

Figure 7: Comparison of calculated effect on final flux uncertainty due to user-variation in net peak area extraction and uncertainty in measurement distance

In each case the overall uncertainty has been calculated as a function of the uncertainty on one parameter while the uncertainty of the other parameter has been set to zero. The uncertainty in the fit

of the intrinsic efficiency, the effective depth of interaction, and the statistical uncertainties on the peak areas provided by the software were left constant in all cases. We can see that as we increase the relative uncertainty in the parameters from 1% to 100%, the effect of uncertainty in measurement distance on the total uncertainty in the flux is a factor of two larger than the effect of user variation in extracted peak areas.

In Figure 7 we see that a 100% uncertainty in the measurement distance results in a 200% relative uncertainty in the calculated photon flux. This follows directly from the inverse square dependence of the solid angle on distance. In the far-field limit we can simplify our view of the solid angle fraction to be the area of the detector face relative to the area of the Gaussian surface illustrated in Figure 3.

$$\frac{Area_{Detector}}{Area_{4\pi}} = \frac{\pi R^2}{4\pi r^2} = \frac{1}{4}\frac{R^2}{r^2}$$

If we double the distance, then the area of our Gaussian surface increases by a factor of 4 and the fraction of that surface covered by the same detector decreases by a factor of 4 (i.e. 200%).

$$\frac{Area_{Detector}}{Area_{4\pi}} = \frac{\pi R^2}{4\pi (2r)^2} = \frac{1}{16}\frac{R^2}{r^2}$$

Because of the above analysis and the fact that the measurement distance *in the field* is often very roughly estimated, we regard the uncertainty in the measurement distance as paramount.

Recommendations

From the above analysis we conclude that the uncertainty in the source-to-detector distance for measurements made in the field is the primary contributor to the uncertainty on the flux of photons into 4π sr. Therefore, emphasizing accurate and precise estimates of this parameter is greatly encouraged when possible. Furthermore, characterizing all fielded detectors in terms of their effective interaction depths for gamma rays of different energies is critical for near-field measurements. Additionally, regular verification of detector efficiency would counter biases due to temporal degradation. Lastly, the development of some means (software) that easily allows the analyst to enter and modify all of these discussed uncertainty contributions into the photon flux calculation is recommended.

Appendix A: Manual Peak Fitting Variation Study

Below are several plots that display the results of the variation that occurs when different analysts obtain the net area for the same peak in the same spectrum.

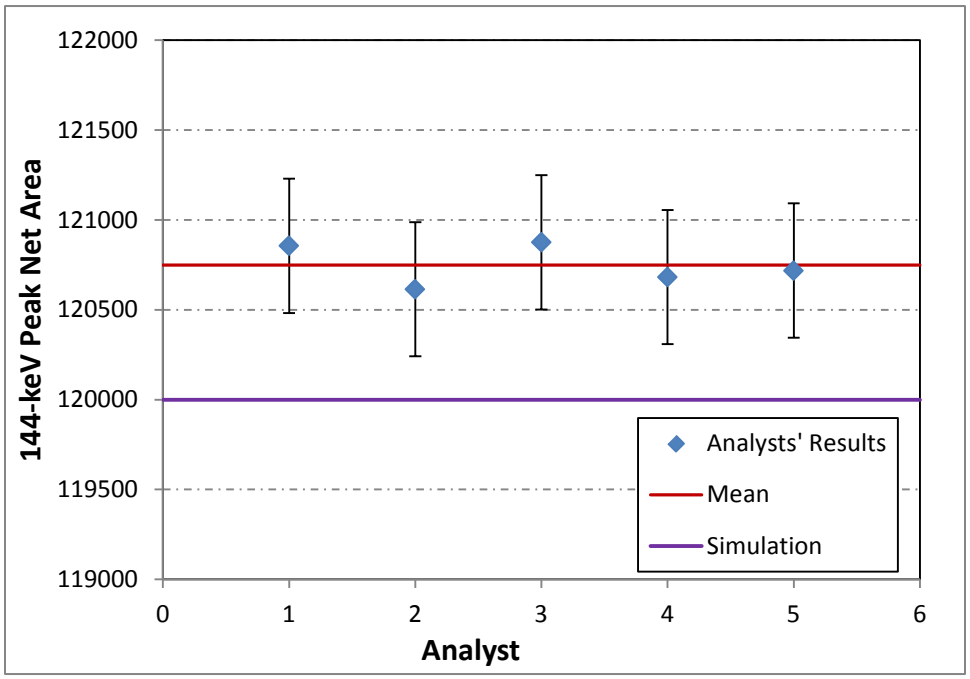

Figure 8: Results for net peak area of 144-keV peak of U-235. (simulated spectrum)

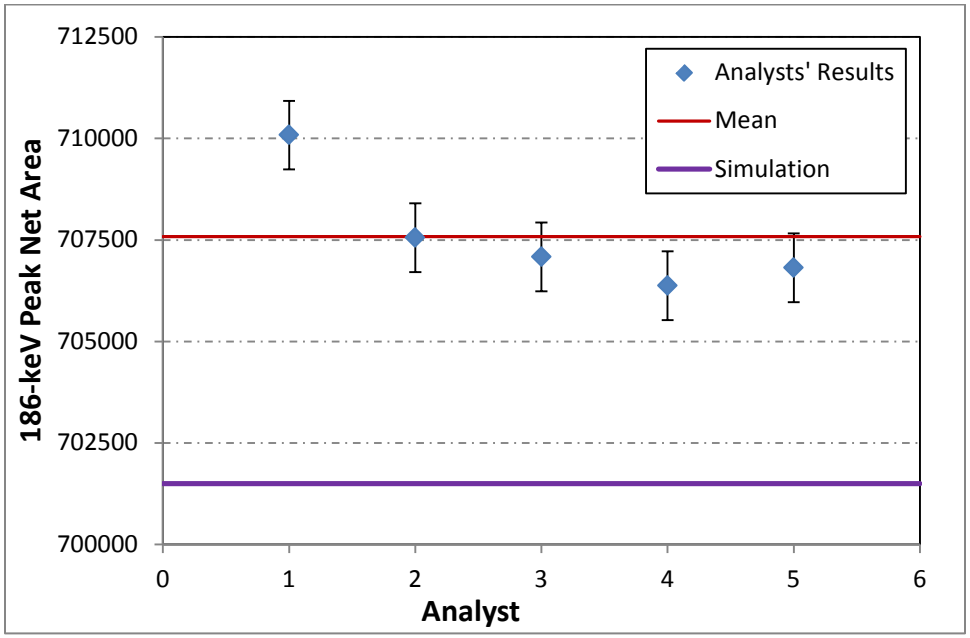

Figure 9: Results for net peak area of 186-keV peak of U-235. (simulated spectrum)

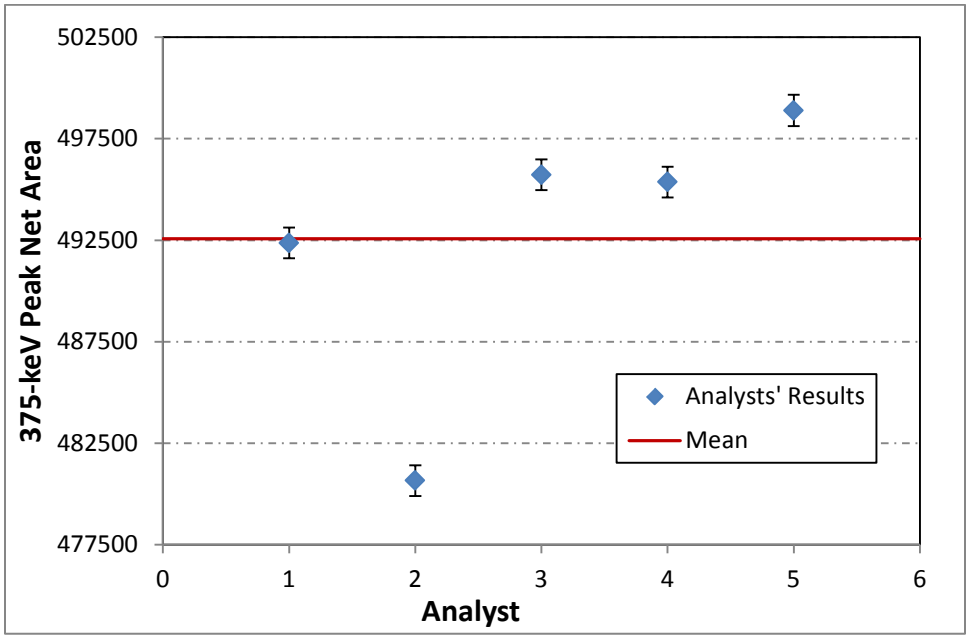

Figure 10: Results for net peak area of 375-keV peak of Pu-239. (real spectrum)

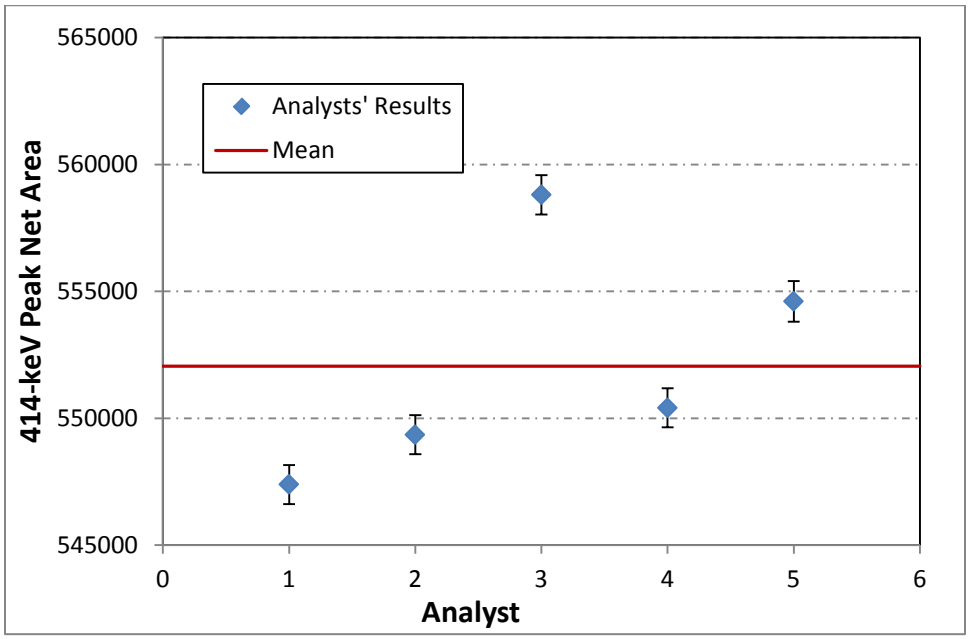

Figure 11: Results for net peak area of 414-keV peak of Pu-239. (real spectrum)

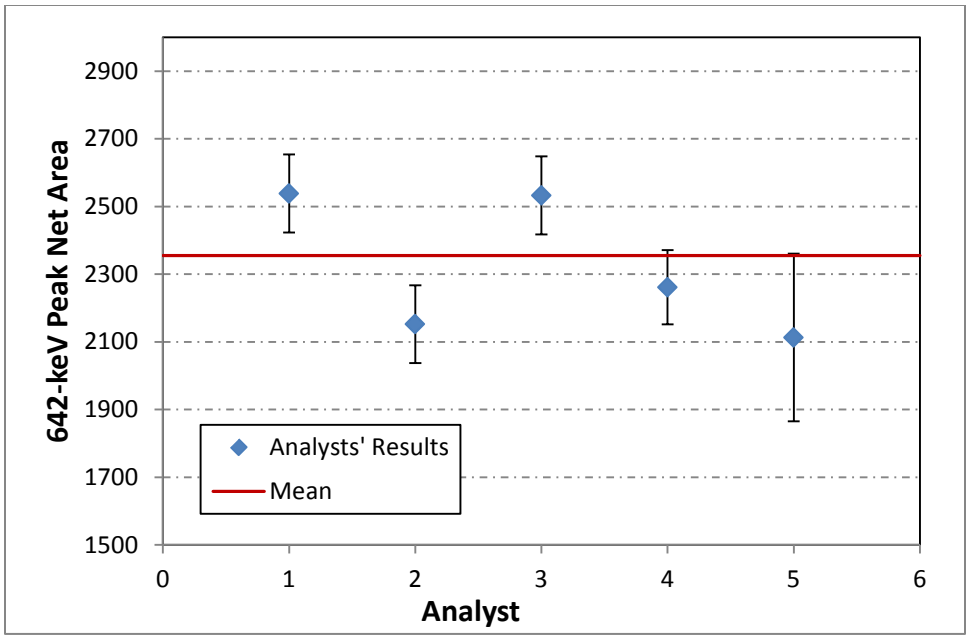

Figure 12: Results for net peak area of 642-keV peak of Pu-240. (real spectrum). The larger error bars on the last data point is likely due to the analyst using a different piece of software than the others.

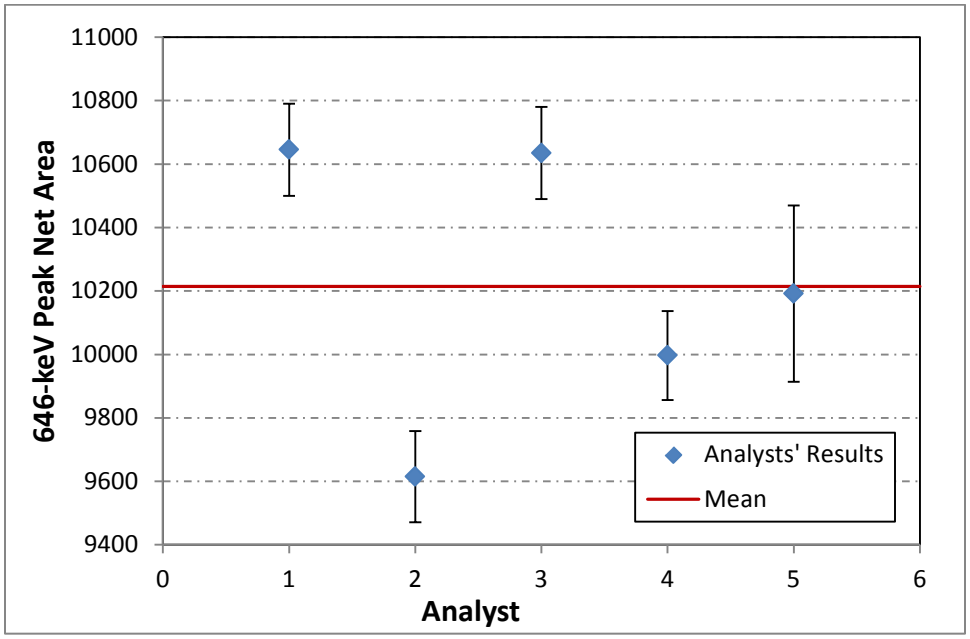

Figure 13: Results for net peak area of 646-keV peak of Pu-239. (real spectrum). The larger error bars on the last data point is likely due to the analyst using a different piece of software than the others.

Appendix B: Detector Intrinsic Efficiency Uncertainty Formalism

Below we examine the derivation of the uncertainty on the intrinsic detector efficiency curve following the method and the primed-nomenclature convention of Bevington[x]. By taking the natural logarithm of both sides we obtain a function that is linear in the parameters.

$$f(E)' = \ln f(E) = c_0 + c_1 \ln E + c_2 (\ln E)^2 + c_3 (\ln E)^3 + c_4 (\ln E)^4 + c_5 (\ln E)^5$$

Partial derivatives, to be used later, will take the following two forms for the original and linearized (indicated by prime notation) functions.

$$\frac{\partial f}{\partial a_k} = e^{(c_0 + c_1 \ln E + \cdots)} (\ln E)^k = f(E)(\ln E)^k$$

$$\frac{\partial f'}{\partial a_k} = (\ln E)^k$$

The data can be fit by employing the multiple regression matrix solution. The elements of the parameter row matrix that result from this approach are

$$a_l = \sum_{k=1}^{m} \left\{ \epsilon_{kl} \sum \left[\frac{1}{\sigma'^2_i} y'_i f'_k(E_i) \right] \right\}$$

Here, y'_i is the value of the log of the i^{th} efficiency data point, σ_i is the uncertainty on that point, $f'_k(E_i)$ is the factor of the function corresponding to the k^{th} parameter evaluated at the i^{th} point, and E_i is the energy of the i^{th} point. ϵ_{kl} is an element of the error or covariance matrix, which contains the variances and covariances of the fitted parameters. The error matrix is obtained by taking the inverse of the curvature matrix $\boldsymbol{\alpha}$,

$$\boldsymbol{\epsilon} = \boldsymbol{\alpha}^{-1}$$

the elements of which are given by

$$\alpha_{lk} = \sum \left[\frac{1}{\sigma'^2_i} f'_l(E_i) f'_k(E_i) \right]$$

Per Bevington[xi], the uncertainties on the data as well as the calculated parameters have been weighted to account for the linearization by the following relations.

$$\sigma'_i = \frac{d(\ln y_i)}{dy} \sigma_i = \frac{\sigma_i}{y_i} \qquad \sigma'_k = \frac{df'}{da_k} \sigma_k = (\ln E)^k \sigma_k$$

Therefore the variance of the intrinsic detector efficiency curve can be written as

$$\sigma_{I_E}^2 = \sum_{k,l} \left(\frac{\partial f}{\partial a_k}\right)\left(\frac{\partial f}{\partial a_l}\right)\sigma_{kl}^2 = \sum_{k,l} f(E)^2 (\ln E)^{k+l}\, \sigma_{kl}^2 = \sum_{k,l} f(E)^2 \sigma_{kl}'^2$$

Here the indices *k* and *l* indicate the variances on the parameters when they are the same and the covariances otherwise. This corresponds to diagonal and off-diagonal elements of the error matrix respectively.

---

[i] Rooney, B.D., http://peakeasy.lanl.gov

[ii] Garner, S.E., LANL, private communication

[iii] "MCNP – A General Monte Carlo N-Particle Transport Code", LANL document LA-UR-03-1987, (2003)

[iv] Garner, S., "PuIsotopics.xls", LANL spreadsheet, March, 2013

[v] T.E. Sampson, T.A. Kelley, and D.T. Vo, "Application Guide to Gamma-Ray Isotopic Analysis Using the FRAM Software," LANL report LA-14018 (2003).

[vi] MCNP Simulations were conducted by Theresa Cutler at LANL

[vii] Myers, S.C., LANL, measurements conducted at the Chemistry and Metallurgical Research Facility, LANL

[viii] Felsher, P.D., LANL, private communication

[ix] D.J. Mitchell, D.R. Waymire. "GADRAS User Manual", Sandia National Laboratory, 2009.

[x] Bevington, P.R., Robinson, D.K.; *Data Reduction and Error Analysis for the Physical Sciences* (McGraw-Hill Higher Education, New York 2003)

[xi] Ibid.